NANOMECHANICAL PHOTOTHERMAL SPECTROSCOPY

An introduction to the EMILIE™ technology

August 4, 2024

1 INTRODUCTION

This white paper introduces EMILIE™, a photothermal infrared spectroscopy technique based on a nanoelectromechanical system (NEMS). EMILIE™, as a nanomechanical photothermal spectroscopy method, is a unique and powerful analytical tool due to its exceptionally wide spectral range, insensitivity to scattering and reflections, efficiency and versatility in sampling a wide variety of materials, the possibility for in-situ thermal desorption analysis, and its exceptional sensitivity at room temperature with a limit of detection (LoD) in the picogram range [1]. This paper further details how this outstanding sensitivity is achieved through the temperature responsivity enhancement of the EMILIE™ sensor chips, the reduced sensitivity to probing light fluctuations (photothermal enhancement), and the low thermomechanical and temperature fluctuation noise limits.

Photothermal spectroscopy represents an analytical technique used to probe the absorption properties of materials through the ensuing non-radiative relaxation processes that generate heat. This method is highly sensitive and non-destructive, making it ideal for studying a broad spectrum of samples. Its general working principle hinges on the detection of thermal changes or mechanical deformations induced by localized heating when a material absorbs light. This is achieved by directing a probing light source at the sample and subsequently measuring the resultant thermal effects using various detection methods.

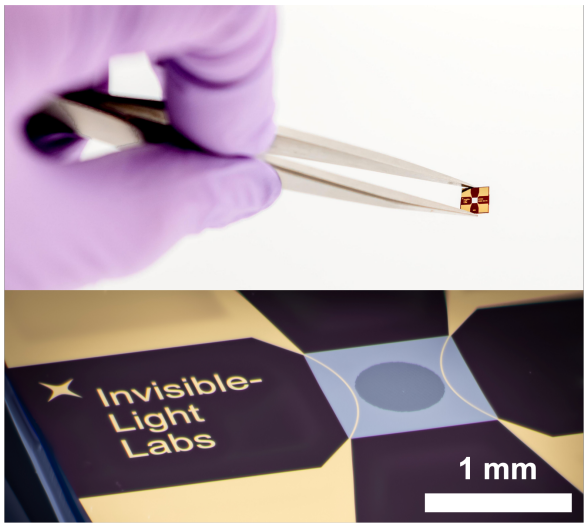


Figure 1: Photographs of the NEMS sensor chip of EMILIE™.

In the case of nanomechanical photothermal sensing with EMILIE™, the heating is measured through a frequency detuning of a highly temperature-sensitive NEMS resonator. The EMILIE™ sensor chip is a nanomechanical drumhead resonator under tensile stress made of a 50 nm thin film of silicon nitride (see Figure 1). The heating-induced thermal expansion causes a reduction in the tensile stress, which strongly affects the drumhead's resonance frequency.

2 SPECTRAL RANGE

EMILIE™ is unique in that the sample is collected directly onto the surface of the nanomechanical resonator, as schematically shown in Figure 2. This con-

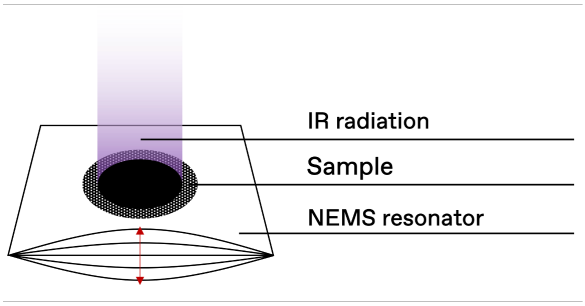


Figure 2: Schematic drawing of the measurement principle of EMILIE™. IR light irradiates a sample that has been collected directly on the surface of a nanoelectromechanical (NEMS) resonator. The photothermal heating of the resonator leads to a measurable detuning of its eigenfrequency.

cept was first introduced in 2013 for the analysis of polymer nanoparticles in the visible (Vis) [2] and infrared (IR) [3] range of the electromagnetic spectrum. Since the sample material directly absorbs the probing light, the nanomechanical photothermal sensing principle is wavelength-agnostic, enabling spectroscopy from the UV [4] all the way to the IR [5, 6, 1]. The sensing principle allows for dispersive spectroscopy, e.g., with a tuneable quantum cascade laser (QCL) [3, 5, 6, 1], and Fourier-transform IR spectroscopy (FTIR), as shown in Figure 3a. Modern FTIR spectrometers are able to span a huge spectral range from the near-IR to the far-IR. Such a wide spectrum is shown in Figure 3b measured with EMILIE™ and covering a spectral range from 6000 cm^{-1} to 30 cm^{-1} (1.67 µm to 333 µm).

3 SCATTERING AND REFLECTANCE

Light scattering and reflections can significantly impact absorption spectroscopy in both reflection and transmission modes, particularly when measuring particulate samples. In transmission spectroscopy, the detector captures less light due to scattering and reflection, creating artifacts in the absorption spectrum. In contrast, EMILIE™, depicted in Figure 6c, is a photothermal method unaffected by these issues, as it measures absorption directly through photothermal heating. This bypasses problems associated with reflections [7], Mie scattering [8, 9, 10], and Rayleigh scattering [11, 12], common in IR and UV-Vis spectroscopy, making EMILIE™ a more reliable technique for accurate spectroscopic analysis of particulate samples.

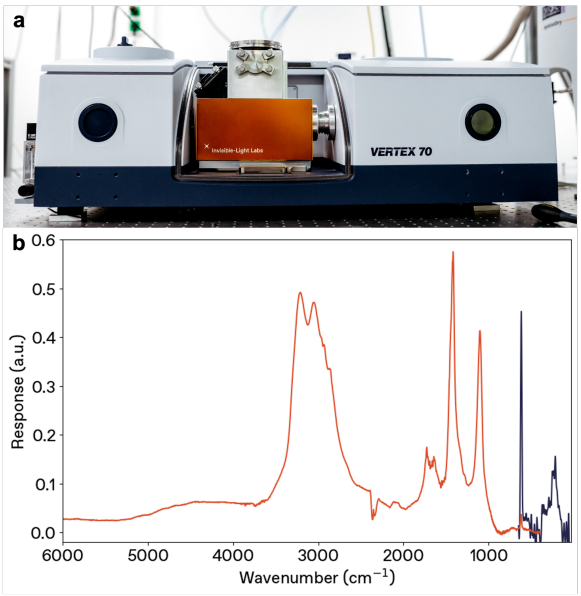


Figure 3: a) Photograph of EMILIE™ in the sample compartment of an FTIR spectrometer. b) FTIR spectrum of rural aerosol (particle size < 700 nm, 15 min sampling time), sampled and measured with EMILIE™ covering a spectral range from 6000 cm^{-1} - 30 cm^{-1} (1.67 µm - 333 µm), measured with a commercial FTIR spectrometer

4 SAMPLING

With EMILIE™, the analyte is sampled directly onto the disposable sensor chip. While this contributes to the exceptional performance of EMILIE™, it further helps to prevent cross-contamination, which is a common issue in trace analysis. The EMILIE™ NEMS resonator is made from silicon nitride, which is a mechanically tough, chemically inert, and temperature-stable material posing essentially no limits to sampling procedures.

Analytes can be stable and semi-volatile compounds that come in the form of a powder, aerosol, dispersion, or solution. The most common sampling techniques with EMILIE™ are drop casting and aerosol impaction. Drop casting, as shown in Figure 4a&b, can be done by hand or with a nanodrop dispenser. Aerosol impaction sampling, shown in Figure 4c&d, aspirates an aerosolized sample through the central perforation of the EMILIE™ chip. This allows sampling of aerosols from 10 nm to 1 µm with a high efficiency [13, 6]. Aerosol impaction sampling can be applied to environmental aerosol, powders, or nebulized dispersions and solutions.

Sampling is not limited to drop casting and aerosol impaction but extends to spin coating, liquid dipping, evaporation, molecular beam deposition, fo-

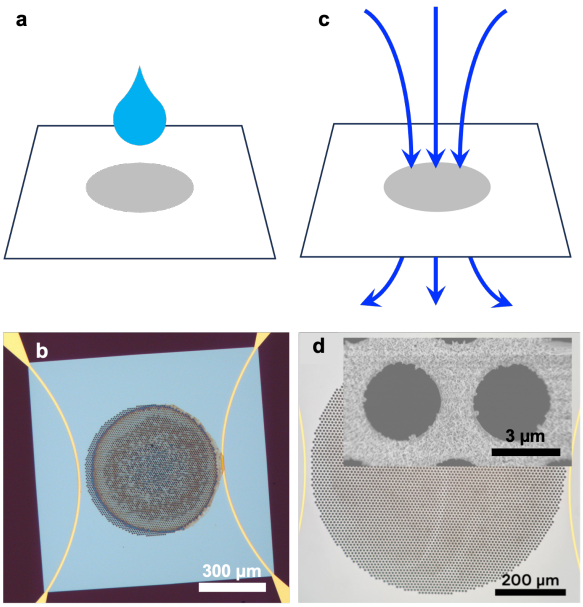


Figure 4: a) Schematic drawing of sample drop casting onto an EMILIE™ chip. b) Photograph of an EMILIE™ chip sampled by drop casting. c) Schematic drawing of sampling through aerosol impaction on an EMILIE™ chip. d) Photograph of an EMILIE™ chip sampled with polymer nanoparticles from a nebulized dispersion through aerosol impaction.

cused electron beam-induced deposition, and physical transfer, e.g., of 2D materials, etc [14].

5 THERMAL DESORPTION

Measurements with EMILIE™ are performed at a pressure of $p < 1 \times 10^{-3}$ mbar. To prevent desorption of semi-volatile analytes during measurement, EMILIE™ allows cooling of the sensor chip during analysis. Conversely, the integrated temperature control also allows heating of the sensor element for the selective thermal desorption of semi-volatile compounds during a measurement [1]. EMILIE™, therefore, allows for in-situ separation of individual compounds from complex samples.

6 SENSITIVITY

While photon detectors can achieve single-photon sensitivity, thermal detectors like bolometers or pyroelectric detectors are typically constrained by electronic noise, including Johnson noise [15]. However, thermomechanical detectors operate on different principles, as they do not rely on electric detection to measure irradiated power. This fundamental difference means that nanomechanical detectors are not limited by electronic noise, which uniquely enables their enhanced sensitivity [16].

The photothermal sensitivity of a nanomechanical resonator is given by its noise-equivalent power (NEP) with units [W/Hz$^{1/2}$] defined as

$$\mathrm{NEP} = \frac{\sqrt{S_y(\omega)}}{\mathscr{R}_P(\omega)}, \tag{1}$$

with the fractional frequency noise power spectral density or frequency stability $S_y(\omega)$ in units of [Hz^{-1}] and the responsivity to absorbed power $\mathscr{R}_P(\omega)$ with units of [W^{-1}] [17].

6.1 Responsivity

The power responsivity of a nanomechanical resonator with an eigenfrequency ω_0 is defined as [17]

$$\mathscr{R}_P = \frac{\partial \omega_0}{\partial P}\frac{1}{\omega_0} H_{th}(\omega) = \frac{\mathscr{R}_T(\omega)}{G} H_{th}(\omega), \tag{2}$$

where $\mathscr{R}_T$ is the frequency responsivity to a change in temperature T and G is the thermal conductance. $H_{th}(\omega)$ is a low-pass transfer function

$$H_{th}(\omega) = \frac{1}{\sqrt{1+\omega^2\tau_{th}^2}}, \tag{3}$$

which drops off for signal frequencies faster than the resonator's thermal time constant $\tau_{th} = C_{th}/G$ with the resonator's heat capacity C_{th}.

Equation (2) shows, that the nanomechanical resonator essentially acts as a thermometer with a temperature responsivity $\mathscr{R}_T$ of the resonator, defined as [17]

$$\mathscr{R}_T = \frac{\partial \omega_0}{\partial T}\frac{1}{\omega_0}. \tag{4}$$

The physical effect underlying $\mathscr{R}_T$ is two-fold: 1) temperature-induced softening of the Young's modulus E, and 2) thermal expansion affecting the tensile stress σ.

In stress-free structures such as beams and plates, the dominant photothermal effect is temperature-induced softening with $\mathscr{R}_T \approx \alpha_E/2$, where α_E is the thermal softening coefficient. Conversely, in pre-stressed structures like strings and drumheads, frequency detuning occurs due to changes in tensile stress through thermal expansion. Here, the temperature responsivity is $\mathscr{R}_T \approx \alpha_{th} E/(2\sigma)$, with α_{th} representing the thermal expansion coefficient of the resonator material [17].

The temperature responsivity of resonators under tensile stress is enhanced by a factor of E/σ, which is generally much greater than one for most materials. This comparison underscores the superiority of prestressed strings and drumhead resonators for temperature sensing over beam and plate resonators. **The silicon nitride drumhead resonators used in EMILIE™ (Figure 1) exhibit a temperature response enhancement factor exceeding 1000.**

The responsivity (2) further scales inversely with the thermal conductance $G = G_{cond} + G_{rad}$, where the operation in vacuum eliminates contributions due to convection. Here, G_{cond} and G_{rad} are the conductances due to conductive and radiative heat transfer, respectively. It has been shown that for the 50 nm thin silicon nitride drumhead resonators, as shown in Figure 1, radiative heat transfer starts to become significant for sizes larger than 1 mm [18, 19].

The responsivity of a square drumhead resonator that is heated evenly can be derived and is given by [17, 20]

$$\begin{aligned}\mathscr{R}_P(\omega) &= \mathscr{R}_T\, G^{-1}\, H_{th}(\omega) \\ &= \frac{\alpha_{th} E}{2\sigma(1-\nu)} \left[2\pi^2\kappa h + 8\varepsilon L^2 \sigma_B T^3\right]^{-1} H_{th}(\omega),\end{aligned} \tag{5}$$

with the resonators Poisson's ratio ν, the thermal conductivity κ, thickness h, emissivity ε, and lateral size L. σ_B is the Stefan–Boltzmann constant.

6.2 Frequency stability

The frequency stability $S_y(\omega)$ in (1) is the sum of the four following noise contributions

$$S_y(\omega) = S_{y,th}(\omega) + S_{y,d}(\omega) + S_{y,T}(\omega) + S_{y,ph}(\omega), \tag{6}$$

which are thermomechanical noise $S_{y,th}(\omega)$, detection noise $S_{y,d}(\omega)$, temperature fluctuation noise $S_{y,T}(\omega)$, and photothermal back action noise $S_{y,ph}(\omega)$ [17]. While there are other noise contributions, such as adsorption-desorption noise, these are the dominating noise sources in nanomechanical resonators to be considered.

Thermomechanical and temperature fluctuation noise are the two fundamental noise sources that ultimately limit the sensitivity of nanomechanical photothermal spectroscopy. These two noise sources can only be reduced through cooling.

6.2.1 Thermomechanical noise

Thermomechanical amplitude fluctuations at resonance

$$S_{z,th} = \frac{4k_B T Q}{m_{eff}\omega_0^3}, \tag{7}$$

with the Boltzmann constant k_B, quality factor Q, and effective resonator mass m_{eff}, translate into phase noise through [21]

$$S_{\varphi,th} = \frac{2}{z_{max}^2} S_{z,th}. \tag{8}$$

The phase noise $S_{\varphi,th}$ can be minimized by maximizing the vibrational amplitude z_{max}, which is typically limited by geometrical nonlinearity.

Finally, the phase noise (8) translates into the fractional frequency noise component $S_{y,th}$ in (6) via

$$S_{y,th} = \frac{S_{\varphi,th}}{\omega_0^2}[H_{\varphi,th}(\omega)]^2 \tag{9}$$

where $H_{\varphi,th}(\omega)$ is a transfer function specific to the oscillator scheme that is used to drive the nanomechanical resonator at resonance. In the case of a self-sustaining oscillator (SSO), which is used in EMILIE™, the transfer function becomes [21]

$$H_{\varphi,th}(\omega) = \frac{1}{\tau_R} H_L(\omega) \tag{10}$$

with the resonator time constant $\tau_R = 2Q/\omega_0$ and the SSO's low-pass filter $H_L(\omega) = (1+\omega^2\tau_L^2)^{-1/2}$ with a filter time constant τ_L. In an SSO, this filter time constant is given by the integration time of the frequency counter [22]. The phase noise to frequency noise transfer function is essentially the same for other oscillator schemes, including phase-locked loops [21].

6.2.2 Detection noise

Detection noise is the noise floor given by the readout system detecting the vibrational motion of the nanomechanical resonator. Hence, like thermomechanical noise, detection noise $S_{z,d}$ can be treated as amplitude noise. As such, the fractional frequency noise component in (6) due to detection noise is given by

$$S_{y,d} = \frac{1}{\omega_0^2}\frac{2}{z_{max}^2} S_{z,d}[H_{\varphi,d}(\omega)]^2 \tag{11}$$

where $H_{\varphi,d}(\omega)$ is the detection noise specific transfer function, given by [21]

$$H_{\varphi,d}(\omega) = \frac{1}{\tau_R}\frac{H_L(\omega)}{H_R(\omega)} \tag{12}$$

with the resonator transfer function with a low-pass characteristic $H_R(\omega) = (1+\omega^2\tau_R^2)^{-1/2}$. The transfer function (12) behaves like a low-pass filter as long as $\tau_L > \tau_R$. However, high-Q resonators can have long time constants, and in that case when $\tau_L < \tau_R$, $H_{\varphi,d}(\omega)$ loses its low pass filter character and starts to increase frequency noise [23]. This underlines the importance of a low-noise readout.

6.2.3 Temperature fluctuation noise

The temperature fluctuation frequency noise $S_{y,T}$ is caused by thermostatistical fluctuations of the resonator temperature according to the fluctuation-dissipation theorem. These temperature fluctuations produce frequency noise via the temperature responsivity $\mathscr{R}_T$ [24, 25]. The fractional frequency noise power spectral density due to temperature fluctuations can be approximated by

$$S_{y,T}(\omega) = \frac{4k_BT^2}{G_{eff}}[H_{th}(\omega)]^2[\mathscr{R}_T(\omega)]^2\,. \tag{13}$$

with the effective thermal conductance for a square drumhead given by [26]

$$G_{eff} = 4\pi h\kappa + 8L^2\varepsilon\sigma_B T^3. \tag{14}$$

The NEP (1) can be estimated based on the thermomechanical and temperature fluctuation noise contributions alone, assuming that photothermal back action noise, as discussed in the following subsection, is insignificant. The NEP for a silicon nitride drumhead resonator is shown in Figure 5.

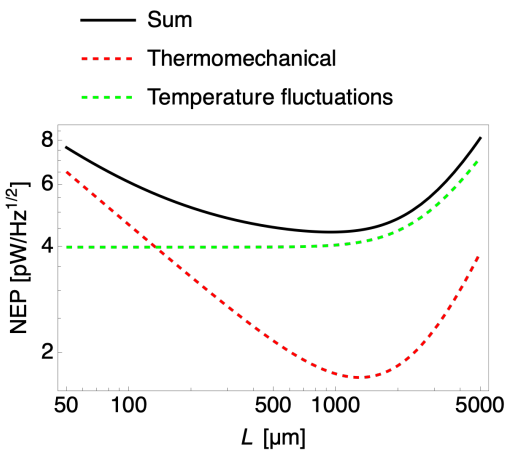


Figure 5: Noise equivalent power model prediction (1) for a square 50 nm thin LPCVD silicon nitride drumhead with a tensile stress of $\sigma = 50$ MPa at room temperature.

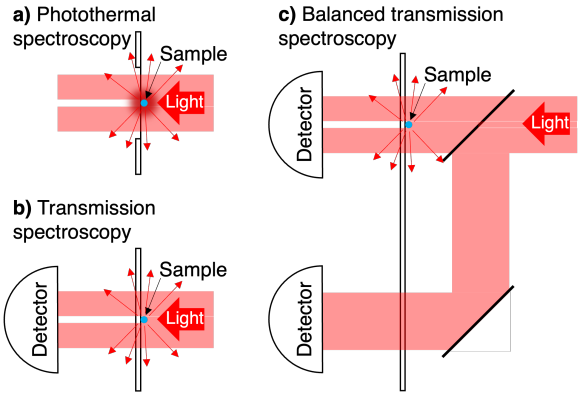


Figure 6: Schematic drawings of a) photothermal spectroscopy, b) transmission spectroscopy, and c) balanced transmission spectroscopy.

6.2.4 Photothermal back-action

The final noise contribution is frequency noise caused by intensity fluctuations in the probing light beam, which can limit the sensitivity of nanomechanical photothermal resonators [23]. Similar to temperature fluctuations, the light intensity fluctuations induce frequency noise through the temperature responsivity $\mathscr{R}_T$. Assuming a continuous wave source with intensity fluctuation power spectral density $S_I(\omega)$ with units [W^2/Hz], the resulting photothermal back-action fractional frequency noise power spectral density is given by

$$S_{y,ph} = \alpha_{abs}^2 S_I(\omega)\mathscr{R}_T^2 \tag{15}$$

with the absorptance α_{abs}.

In nanomechanical photothermal spectroscopy, this back action noise (15) scales with the absorptance α_{abs}, which typically is a lot smaller than one. In other words, the sensor only captures the small intensity noise fraction of the absorbed light, as schematically depicted in Figure 6a. This stands in contrast to traditional transmission spectroscopy, as depicted in Figure 6b, where the detector captures the intensity noise of the transmitted $T \approx 1-\alpha_{abs}$ light. Comparing the signal-to-noise ratios of photothermal $SNR_{ph} \approx \alpha_{abs}/[\alpha_{abs}S_I(\omega)]$ and transmission $SNR_{tr} \approx \alpha_{abs}/[TS_I(\omega)]$ spectroscopy for case that $\alpha_{abs} \ll 1$ shows the so-called "photothermal en-

hancement"

$$\frac{SNR_{ph}}{SNR_{tr}} \approx \frac{1}{\alpha_{abs}} \gg 1. \tag{16}$$

For small samples with a small absorptance and a noisy light source, such as a QCL, photothermal spectroscopy has a signal-to-noise ratio that is enhanced by a factor of $1/\alpha_{abs} \gg 1$ compared to transmission spectroscopy.

While intensity noise is typically negligible in thermal light sources, it can pose a problem in high-power mid-IR QCL. It has been shown that such classical noise can be effectively eliminated using a balanced transmission scheme [27], as illustrated in Figure 6c. Photothermal spectroscopy inherently provides intensity noise suppression comparable to balanced transmission spectroscopy but without the additional complexity of a balanced setup.

6.3 Limit of Detection

The limit of detection (LoD) can be estimated from the NEP and the photothermal heating induced by a sample for a given probing light power. The number of molecules n that give a signal equivalent to the noise can be calculated from $n = NEP/(IA)$, with the probing light irradiance I in units of [W/m^2] and the absorption cross-section of a single molecule A in unit of [m^2].

For the estimated $NEP \approx 4$ pW/Hz$^{1/2}$, as shown in Figure 5, the LoD can be estimated for a low-noise thermal light source with a power of 100 nW and a focal beam diameter of 1 mm^2. For a protein sample, e.g., BSA with a molecular mass of 66.5 kDa and an absorption cross-section of 7.3×10^{-20} m^2 at a wavelength of 6 µm [28], this results in an estimated LoD (3 sigma) of 180 pg for an integration time of 1 second. This is a good approximation for the LoD of EMILIE™ with an FTIR. This can be improved further when using EMILIE™ together with a strong mid-IR QCL, resulting in LoDs in the single-digit picogram range [1].

REFERENCES

[1] Niklas Luhmann, Robert G. West, Josiane P. Lafleur, and Silvan Schmid. Nanoelectromechanical infrared spectroscopy with in situ separation by thermal desorption: Nems-ir-td. ACS Sensors, 8:1462–1470, 4 2023.

[2] Tom Larsen, Silvan Schmid, Luis G Villanueva, and Anja Boisen. Photothermal Analysis of Individual Nanoparticulate Samples Using Micromechanical Resonators. ACS Nano, 7(7):6188–6193, 2013.

[3] Shoko Yamada, Silvan Schmid, Tom Larsen, Ole Hansen, and Anja Boisen. Photothermal infrared spectroscopy of airborne samples with mechanical string resonators. Analytical Chemistry, 85:10531–10535, 11 2013.

[4] Jan N. Kirchhof, Yuefeng Yu, Denis Yagodkin, Nele Stetzuhn, Daniel B. de Araújo, Kostas Kanellopulos, Samuel Manas-Valero, Eugenio Coronado, Herre van der Zant, Stephanie Reich, Silvan Schmid, and Kirill I. Bolotin. Nanomechanical absorption spectroscopy of 2D materials with femtowatt sensitivity. pages 0–7, 2023.

[5] Alina J. Andersen, Shoko Yamada, E. K. Pramodkumar, Thomas L. Andresen, Anja Boisen, and Silvan Schmid. Nanomechanical IR spectroscopy for fast analysis of liquid-dispersed engineered nanomaterials. Sensors and Actuators, B: Chemical, 233:667–673, 2016.

[6] Maksymilian Kurek, Matthias Carnoy, Peter E. Larsen, Line H. Nielsen, Ole Hansen, Thomas Rades, Silvan Schmid, and Anja Boisen. Nanomechanical Infrared Spectroscopy with Vibrating Filters for Pharmaceutical Analysis. Angewandte Chemie, 129(14):3959–3963, 2017.

[7] Paul Bassan, Hugh J Byrne, Joe Lee, Franck Bonnier, Colin Clarke, Paul Dumas, Ehsan Gazi, Michael D Brown, Noel W Clarke, and Peter Gardner. Reflection contributions to the dispersion artefact in ftir spectra of single biological cells. Analyst, 134(6):1171–1175, 2009.

[8] Paul Bassan, Hugh J Byrne, Franck Bonnier, Joe Lee, Paul Dumas, and Peter Gardner. Resonant mie scattering in infrared spectroscopy of biological materials–understanding the 'dispersion artefact'. Analyst, 134(8):1586–1593, 2009.

[9] Paul Bassan, Achim Kohler, Harald Martens, Joe Lee, Hugh J Byrne, Paul Dumas, Ehsan Gazi, Michael Brown, Noel Clarke, and Peter Gardner. Resonant mie scattering (rmies) correction of infrared spectra from highly scattering biological samples. Analyst, 135(2):268–277, 2010.

[10] Alexandre Dazzi, Ariane Deniset-Besseau, and Peter Lasch. Minimising contributions from scattering in infrared spectra by means of an integrating sphere. Analyst, 138(14):4191–4201, 2013.

[11] J Zachary Porterfield and Adam Zlotnick. A simple and general method for determining the protein and nucleic acid content of viruses by uv absorbance. Virology, 407(2):281–288, 2010.

[12] Matthias Rüdt, Philipp Vormittag, Nils Hillebrandt, and Jürgen Hubbuch. Process monitoring of virus-like particle reassembly by diafiltration with uv/vis spectroscopy and light scattering. Biotechnology and bioengineering, 116(6):1366–1379, 2019.

[13] Silvan Schmid, Maksymilian Kurek, Jens Q. Adolphsen, and Anja Boisen. Real-time single airborne nanoparticle detection with nanomechanical resonant filter-fiber. Scientific Reports, 3:3–7, 2013.

[14] Robert G West, Kostas Kanellopulos, and Silvan Schmid. Photothermal microscopy and spectroscopy with nanomechanical resonators. The Journal of Physical Chemistry C, 127(45):21915–21929, 2023.

[15] Antoni Rogalski. Infrared and Terahertz Detectors, Third Edition. CRC Press, jan 2019.

[16] H. H. Cary. Infrared radiation detector employing tensioned foil to receive radiation, 1969. US Patent 3457412A.

[17] Silvan Schmid, Luis Guillermo Villanueva, and Michael Lee Roukes. Fundamentals of nanomechanical resonators, 2nd edition. Springer International Publishing AG Switzerland, 2023.

[18] Markus Piller, Pedram Sadeghi, Robert G West, Niklas Luhmann, Paolo Martini, Ole Hansen, and Silvan Schmid. Thermal radiation dominated heat transfer in nanomechanical silicon nitride drum resonators. Applied Physics Letters, 117(3):034101, 2020.

[19] Chang Zhang, Mathieu Giroux, Thea Abdul Nour, and Raphael St-Gelais. Radiative heat transfer in freestanding silicon nitride membranes. Physical Review Applied, 14(2):024072, 2020.

[20] Kostas Kanellopulos, Robert G. West, and Silvan Schmid. Nanomechanical photothermal spectroscopy of individual nanorods. in preparation: https://arxiv.org/abs/2305.05287, 2023.

[21] Hajrudin Bešić, Alper Demir, Johannes Steurer, Niklas Luhmann, and Silvan Schmid. Schemes for tracking resonance frequency for micro-and nanomechanical resonators. Physical Review Applied, 20(2):024023, 2023.

[22] Hajrudin Bešić, Alper Demir, Veljko Vukićević, Johannes Steurer, and Silvan Schmid. Adaptable frequency counter with phase filtering for resonance frequency monitoring in nanomechanical sensing. IEEE Sensors Journal, 2024.

[23] Pedram Sadeghi, Alper Demir, Luis Guillermo Villanueva, Hendrik Kahler, and Silvan Schmid. Frequency fluctuations in nanomechanical silicon nitride string resonators. Physical Review B, 102, 12 2020.

[24] John R Vig and Yoonkee Kim. Noise in microelectromechanical system resonators. IEEE transactions on ultrasonics, ferroelectrics, and frequency control, 46(6):1558–1565, 1999.

[25] A. N. Cleland and M. L. Roukes. Noise processes in nanomechanical resonators. Journal of Applied Physics, 92(5):2758–2769, 2002.

[26] Kostas Kanellopulos, Friedrich Ladinig, Stefan Emminger, Paolo Martini, Robert G West, and Silvan Schmid. Comparative analysis of nanomechanical resonators: Sensitivity, response time, and practical considerations in photothermal sensing. arXiv preprint arXiv:2406.03295, 2024.

[27] Christopher K Akhgar, Georg Ramer, Mateusz Żbik, Artur Trajnerowicz, Jarosław Pawluczyk, Andreas Schwaighofer, and Bernhard Lendl. The next generation of ir spectroscopy: Ec-qcl-based mid-ir transmission spectroscopy of proteins with balanced detection. Analytical Chemistry, 92(14):9901–9907, 2020.

[28] Andreas Schwaighofer, Christopher K Akhgar, and Bernhard Lendl. Broadband laser-based mid-ir spectroscopy for analysis of proteins and monitoring of enzyme activity. Spectrochimica Acta Part A: Molecular and Biomolecular Spectroscopy, 253:119563, 2021.